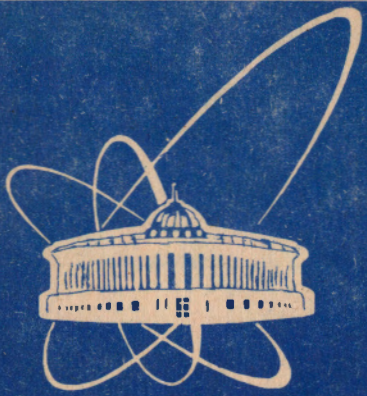

СООБЩЕНИЯ
ОБЪЕДИНЕННОГО
ИНСТИТУТА
ЯДЕРНЫХ
ИССЛЕДОВАНИЙ

Дубна

E14-97-85

MEASUREMENTS OF RESIDUAL STRAINS IN A SHAPE WELDED STEEL TUBE BY NEUTRON AND X-RAY DIFFRACTION METHODS

1997

V.L.Aksenov, A.M.Balagurov, Yu.V.Taran
Frank Laboratory of Neutron Physics, JINR, Dubna, Russia

M.Kröning, J.Schreiber
Fraunhofer Institute for Nondestructive Testing, Saarbrucken, Germany

P.Mikula, P.Lukas, M.Vrana
Nuclear Physics Institute, Rez, Czech Republic

G.D.Bokuchava
Institute for Nuclear Research, RAS, Moscow, Russia

H.Kockelmann
MPA, Stuttgart University, Germany

K.Macek, J.Jenik
Czech Technical University, Prague, Czech Republic

1. INTRODUCTION

Shape welding [1] is an interesting alternative method, but the existence of uncontrollable residual stress distributions in welded materials prevents its wide application. On the other hand, shape welded ferritic layers on austenitic tubes can help suppress stress corrosion because these layers produce the compressive stress states on the austenitic tube. The analysis of residual stresses through the ferritic weld into the austenitic material can be helpful for the optimization of the corresponding welding technique [2].

For many years, different non-destructive testing methods, such as X-ray diffraction, ultrasonic scanning, as well as various magnetic techniques, e.g., based on the Barkhausen noise effect, have been used to investigate internal mechanical stresses in materials [3],[4]. However, the application of these methods is restricted [3]. For example, X-ray scattering or magnetic methods allow us to investigate only stresses near the surface of the material because of the small penetration depth of these methods.

Stress investigations by neutron diffraction occupy a special position in non-destructive testing [5],[6]. First, because neutrons penetrate into materials to the depth 2-4 cm for steel and over 10 cm for aluminium. The strain caused by internal stresses is of the order 10^{-3} - 10^{-5} and requires a higher resolution of the diffractometer, i.e. $\Delta d/d \approx 0.3\%$. At present, in the world, about twenty neutron diffractometers at stationary reactors and pulsed neutron sources are operating for such investigations. For scattering experiments, the 90° setup is optimal, because its most suitable gauge volume in the form of a rectangular parallelepiped is easy to be separated using collimators and masks. The 90° scattering geometry can be realized most naturally, with the time-of-flight technique. Also this technique has the possibility of measuring simultaneously a large number of reflexes. The changes in the lattice spacing averaged over the measured volume and along the reflex-direction [hkl] can be obtained by measuring the Bragg-peak shifts. Investigations of all available reflexes gives information about the strain-stress anisotropy and II. kind residual stresses [7]. Microstresses can be investigated by measuring the shape of the diffraction peaks.

In this article, the stress state in shape welded tubes is analyzed by the nondestructive neutron and X-ray diffraction methods and is compared to the data obtained by the destructive turning out technique and theoretical predictions of calculations by the finite element method.

2. THE SAMPLE

The investigated sample was prepared by MPA, Stuttgart [2]. Seven layers of ferritic steel with 135 welding traces and a total length of 1100 mm were welded on a 15 mm thick austenitic steel tube with an outer radius of 148 mm. The outer radius of the manufactured two-layer tube was 168 mm. The chemical composition of the layers is given in Table 1.

Table 1. The chemical composition of the layers welded on the steel tube

Layer	Steel	C	Si	Mn	P	S
Inner layer (austenite, γ-phase)	X6CrNiTi 18 10	0.06	0.44	1.77	0.031	0.003
Outer layer (ferrite, α-phase)	3NiMo 1UP	0.06	0.12	1.03	0.021	0.004

Cr	Ni	Mo	V	Al	Cu	W	Co	Ti
17.0	10.6	0.34	0.07	0.20	0.32	0.05	0.12	0.39
0.52	1.02	0.57	<0.01	0.01	0.06	<0.01	0.03	<0.01

For measurements at neutron sources, a test specimen was prepared (Fig. 1). First, a segment was cut from the manufactured tube (200 mm long, 70° of arc circumference). With the extensiometers in the middle of the segment oriented in the axial and circumferential (tangential) direction, the effect of stress release was measured at the inner and outer edges of the segment (see Table 2). Because of the limited beam time for the HRFD diffractometer, the investigated sample was further simplified by cutting a smaller segment as shown in Fig. 2. The analysis of the whole segment will be carried out in subsequent experiments.

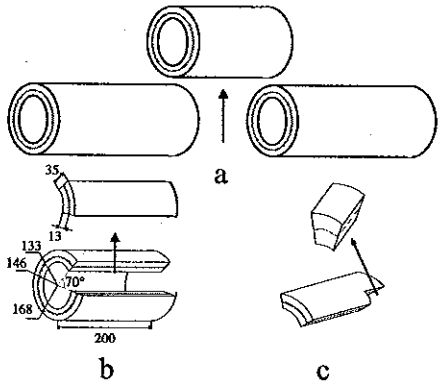

Fig. 1. Scheme of the sample preparation procedure for neutron measurements: a - cutting out the 200 mm long tube, b - cutting out the 70° circumference segment from the tube, c - cutting out the sample from the segment.

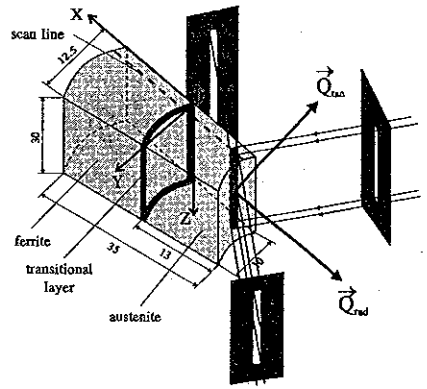

Fig. 2. The investigated sample and the (x,y,z) sample-related coordinate system.

Table 2. Stress release results for the truncated tube segment

Strain/ Stress	Inner side		Outer side	
	axial	tangential	axial	tangential
$\Delta\varepsilon$ [10^{-4}]	-2.7	21.3	4.3	-15.3
$\Delta\sigma$ [MPa]	80 (4)	-450 (2)	6 (3)	307 (2)

In [2], the detail characteristics of the tube material are given. Most parameters of materials, including elastic constants, tensile strength, and hardness were obtained by cutting test specimens. Austenitic steel was found to have E=176 GPa, ν=0.3, R_m=536 MPa and the hardness 155 HV10. For a ferritic welded material, the average values E=205 GPa, ν=0.3, R_m=695 MPa and the hardness 200 HV10 far from the transition region, where its value reaches 380 HV10 were found.

By destructive testing methods, such as the hole drilling and turning out techniques residual stresses were determined in different points of the tube. Later, these results will be compared to the results of neutron diffraction investigations.

For microstructure and microhardness investigations, six 14x14x14 mm cubic samples of submerged arc weldments were prepared for metalographic investigations. The sample surfaces were polished mechanically. Analogous macrostructures were revealed in all investigated cases. The austenitic part of the tube almost unetched by means of a Villela-Bain etchant (0.5 g picral acid, 3 ml hydrochloric acid, 96 ml ethanol), several layers of fairly well etched weld metal were observed.

The microstructure was investigated with the ZEISS-NEOPHOT 32 instrument by the light microscopy method. In the micrographs obtained by bright field illumination, one can see very gently etched austenitic metal (Fig. 3) and several ferritic layers, whose microstructure consists of acicular ferrite, also called low-carbon bainite (Figs. 3-5). While the transitional zone between the adjacent ferritic layers is microstructuraly continuous (Fig. 4), a dark eutectic type microconstituent is observed on the phase boundary between the austenitic tube and the first ferritic layer (Figs. 3, left and 5, left). This microconstituent is also observed on the preceding austenitic grain boundaries in the first ferritic layer (Fig. 5, right). The wave-dispersive microanalysis of the chemical composition performed using a CAMEBAX device showed that this dark microconstituent was basically created by oxides, although the possible presence of some carbide phases was also considered.

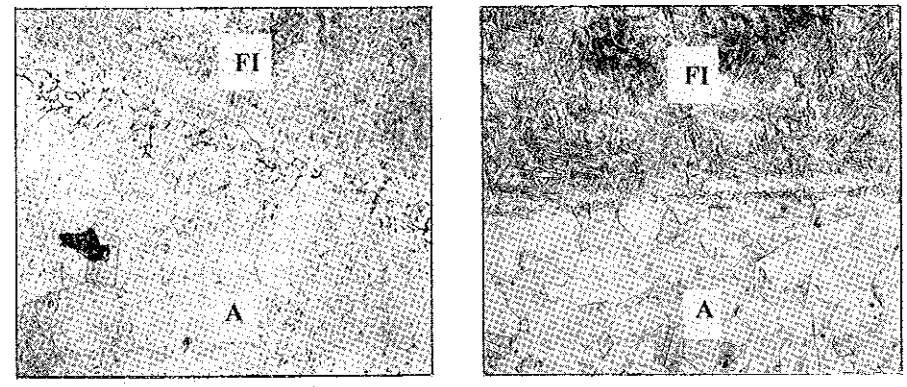

Fig. 3. The micrographs of the boundary between the austenitic tube and the first ferritic layer: left - sample no.1, right - sample no.3.

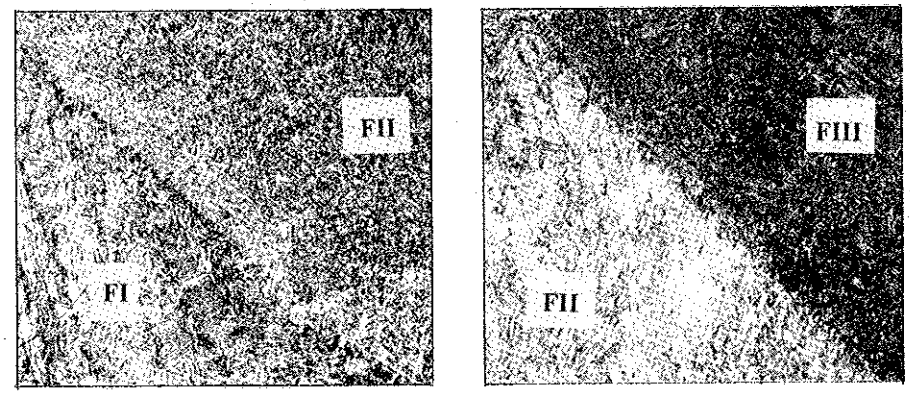

Fig. 4. The micrographs of the ferritic layers of sample no.1: left - the boundary between the first and second layers, right - the boundary between the second and third layers.

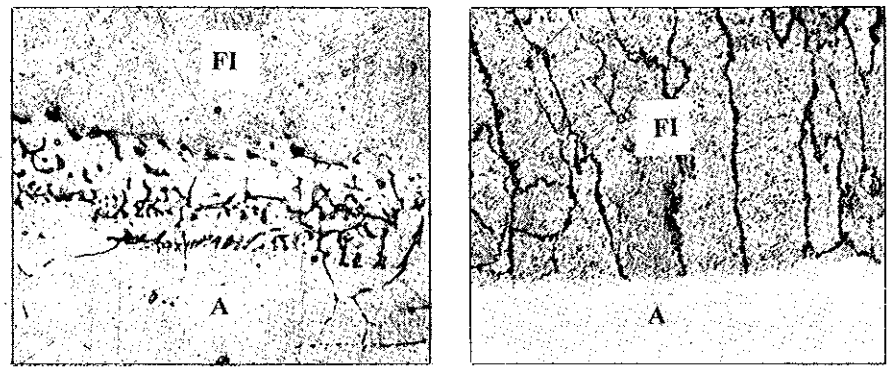

Fig. 5. The micrographs of the boundary between the austenitic tube and the first ferritic layer of sample no.6: left - the magnification 250X, right - 100X.

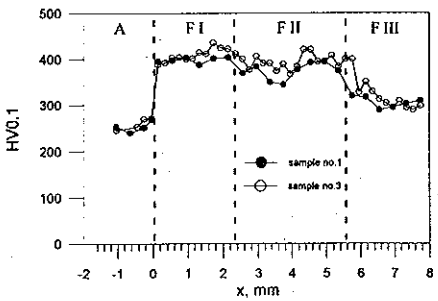

Fig. 6. The dependence of the microhardness HV0.1 on the x coordinate: A - the austenitic tube, FI, FII and FIII - the ferritic layers.

To conduct microhardness measurements, a LECO INSTRUMENT tester was used with an applied load of 0.981 N. Indentations were aligned with the x-direction. The distance between the neighbouring indentations was either 0.4 mm (sample no.1) or 0.2 mm (sample no.3). The results are shown in Fig. 6. The microhardness of the austenitic tube was about 245 HV0.1, but the zone containing the mentioned oxide microconstituent was slightly harder (270 HV0.1). A pronounced increase in the microhardness was detected within the first ferritic layer (395 to 403 HV0.1) for sample 1 and a sudden drop in the microhardness within the third ferritic layer was observed for both samples. At the same time, the third layer was softer than the other ferritic layers. This means that the third layer was cooled more slowly during the welding process. As a result, we can conclude that good agreement exists between the thickness of the layers observed with a naked eye and the appearance of hardness on the plot HV vs. the x coordinate.

3. NEUTRON MEASUREMENTS

Diffractometers. The neutron strain measurements of the described sample were performed on the High Resolution Fourier Diffractometer (HRFD) at the IBR-2 pulsed reactor in Dubna (Fig. 7) [8] and the TKSN-400 triple-axis diffractometer at the LWR-15 stationary reactor in Rez (Fig. 8) [9].

The HRFD is equipped with a Fourier chopper. This chopper modulates the IBR-2 thermal neutron pulse with the initial width 320 μs. The modulation is performed with the frequency from 0 to 150 kHz. The resulting minimum width is 7 μs. The neutron energy is determined by the reverse

time-of-flight method on the 20 m flight path. At present, HRFD has four detectors: DOR-1 and DOR-2 backscattering detectors at the scattering angle ±152° and DPR-1 and DPR-2P detectors at the angles ±90°. Although DORs are mainly used for precision structural investigations with the resolution about 0.1%, a number of experiments to measure residual stresses in different materials were conducted with this detector as well (e.g. [10], [11]). Two other detectors are mainly used for residual stress measurements. The resolution Δd/d of these detectors (d is the lattice interplane spacing and Δd is the half width of the Bragg reflex) was 0.4-0.5 % at d=2 Å at the maximum modulation frequency 50 kHz.

The TKSN-400 was equipped with a bent Si single crystal monochromator and an analyzer. This allowed a high luminosity and resolution to be obtained (Δd/d=0.25 % for d=2 Å).

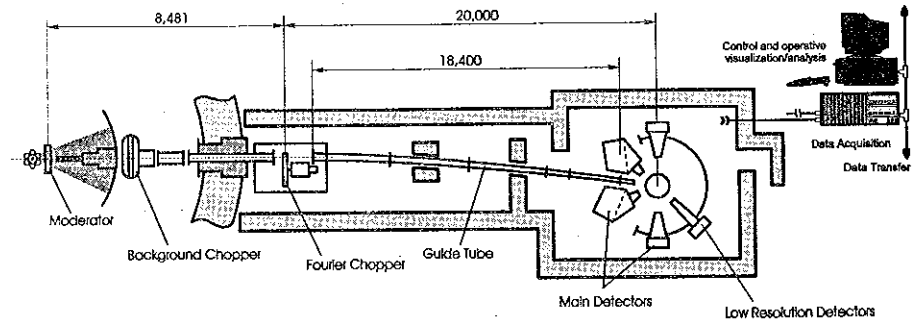

Fig. 7. The scheme of the HRFD neutron diffractometer at the IBR-2 reactor (Dubna).

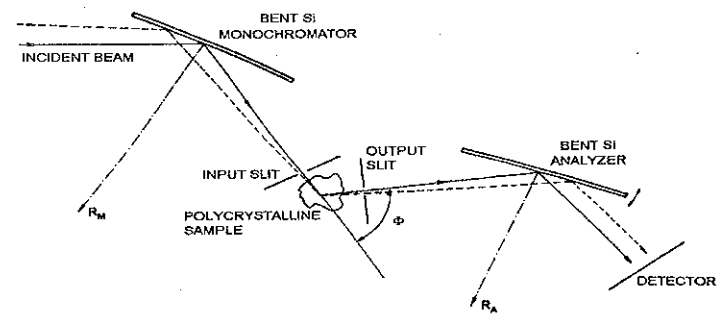

Fig. 8. The scheme of the TKSN-400 neutron diffractometer at the LWR-15 reactor (Rez).

Measurements. The strain in the investigated sample was primarily scanned in the radial direction to the depth 2.5 mm from the surface of the sample on the TKSN-400 using a Huber goniometer. The radial strain component (the Q-scattering vector is radially directed along the x-axis in Fig. 2) and the tangential strain component (the Q-vector is tangentially directed along the y-axis in Fig. 2) were measured by forming the gauge volume by the Cd-masks in the direct neutron beam (1.5 mm wide by 25 mm high) and the diffracted neutron beam (2 mm wide). To measure the axial strain component (the Q-vector is axially directed along the z-axis in Fig. 2), the height of the beam was decreased by a factor of 2.5. The (111) and (110) Bragg reflexes were used to measure

strain in the austenitic (γ-phase) and ferritic (α-phase) layers, respectively. In the vicinity of the transitional layer, changes in the d-interplane spacing up to 0.2% of its value at the sample edges in the radial direction were observed.

Strain scanning to the depth 2 mm from the surface of the sample was conducted on HRFD with the help of a (x,y,z,ω)-translator. Both radial and tangential strain components were measured simultaneously using two detectors at the scattering angles ±90°. To form the direct beam, a boron nitride (BN) diaphragm with a slit 2 mm wide by 20 mm high was installed at the exit of a mirror neutron-guide. To set the scattered beams at ±90°, BN-diaphragms with the 2 mm slit width were installed at the distance 42 mm from the center of the diffractometer. The gauge volumes formed by these diaphragms were 2.1×4.5×19.4 and 2.1×2.6×19.4 mm^3 for DPR-1 and the DPR-2P detectors, respectively.

In Figs. 9 and 10, DPR-1 diffraction spectra from the inner and outer sides of the tube are shown. The characteristic minimums at the peak bases are determined of the particularity of the spectra's registration on Fourier diffractometer. In both cases, four reflexes were observed in the γ- as well as in the α-phases. Processing of these spectra by the Rietveld method (MRIA program [12]) revealed noticeable texturation of the sample in the γ-phase. The (200) Bragg reflex over the interval of channels from 1710 to 2000 in Fig. 9 had the intensity nearly 8 times higher than the calculated value for randomly oriented grains. This peak was omitted in the fitting procedure. Practically no texturation was found in the α-phase.

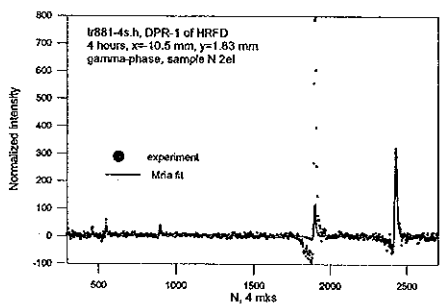

Fig. 9. The spectrum of the investigated sample in the γ-phase measured with DPR-1 for 4 hours. As a result of MRIA fitting, the cubic lattice constant a=3.5909(1) Å was obtained.

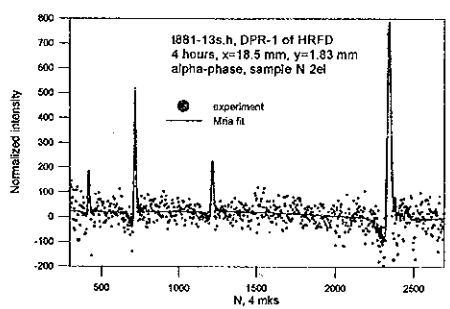

Fig. 10. The spectrum of the investigated sample in the α-phase measured with DPR-1 for 4 hours. The obtained cubic lattice constant was a=2.8673(1) Å.

Results. Finding of all available peak positions in the measured spectra allows strain to be evaluated, if the stress-free reference values of the lattice spacing d_0^{hkl} are known. However, there were some difficulties in determining the values of these quantities. We tried to determine d_0^{hkl} using powder samples from the austenitic steel part of the tube as well as welded material. It looked as if these powders did not provide stress-free reference states of the tube constituents. Filling and annealing of these materials might cause structural changes and falsify the d_0^{hkl}-values, e.g. the martensitic phase could be built during the cold forming process of austenitic steel. In the welded ferritic material the carbon content can be changed and hence, d_0^{hkl} can be altered. In such an unclear situation, the so-called boundary (edge) values measured far away from the transitional layer were used as free-stress spacings (see Table 3).

Table 3. The d_0 free-stress spacings and the Γ orientation factor for the α- and the γ-phases

α-phase			γ-phase		
hkl	d	Γ	hkl	d	Γ
110	2.0270(5)	1/4	111	2.0728(3)	1/3
200	1.4331(3)	0	200	1.7956(2)	0
211	1.1703(2)	1/4	220	1.2695(2)	1/4
220	1.0135(2)	1/4	311	1.0831(2)	19/121

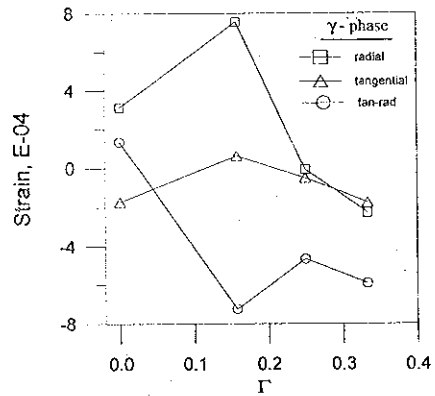

Fig. 11. The dependence of the strain values in the radial and tangential directions on the orientation factor Γ for the inner wall of the austenitic steel tube (X=-10.5 mm). The d_0^{hkl} are calculated from the lattice constant obtained by Rietveld fitting (see Fig. 9). In the position X=-5.5 mm, the difference between two strain components is shown.

To clarify the role of grain interaction stresses (II. kind residual stress - see [13]), the character of the dependence of the strain on the orientation factors Γ is investigated. In the case of the cubic lattice, the orientation factor is $\Gamma=(h^2k^2+h^2l^2+k^2l^2)/(h^2+k^2+l^2)$. As is seen from Fig. 11, the strain values vary nonlinearly as the factor Γ varies. This points to the presence of strong grain interaction stresses. Unfortunately, this circumstance causes some difficulties in the analysis of the macroscopic stress state, i.e. the I. kind residual stress is difficult to be extracted in this case.

Fig. 12 and 13 show the estimated results for strain in the ferritic part of the investigated shape welded tube (α-phase) and for the austenitic region of the specimen (γ-phase). The strain values for different orientations of the scattering vector **Q** available from the neutron diffraction experiment on HRFD, are presented.

Because of the difficulties in measuring microstresses, the choice of reflexes for the evaluation of macrostresses in each phase is a subject for discussion. In the following, pairs of reflexes for the α- and γ-phases with equal orientation factors Γ will be picked up (see Table 3). Thus, the appearance of uncontrollable fluctuations due to plastic anisotropy will be prevented. Good results for all scanned positions were obtained only for (200)-reflexes (Γ=0). Therefore, these reflexes will be used in the further discussion.

Before analyzing macrostresses, a comparison of the strain values measured with the HRFD and TKSN-400 is carried out (Fig. 14). Good agreement was obtained for the radial components using (110)- and (111)-reflexes. The agreement was worse for the tangential components. This might be connected with the change in the gauge volume orientation in the sample when passing from measuring of the radial to the tangential component accompanied by rotation of the sample by 90°. On the other side, uncertainty in the determination of d_0^{hkl} can be explained, first of all, by deviations of strain values on the ferritic part of the tube.

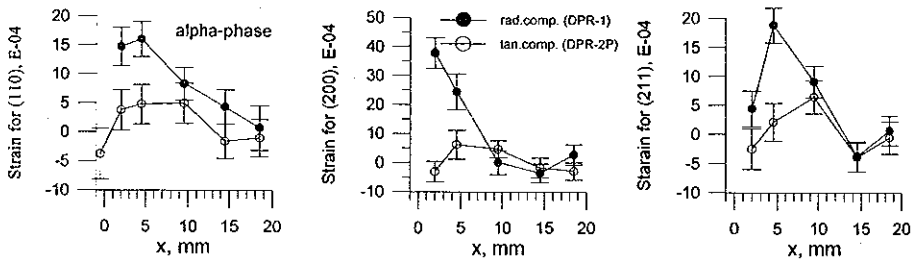

Fig. 12. The dependence of the radial and tangential components of the strain ε on the location of the gauge volume x for the reflexes measured from the investigated sample in the α-phase with the DPR-1 and DPR-2P detectors.

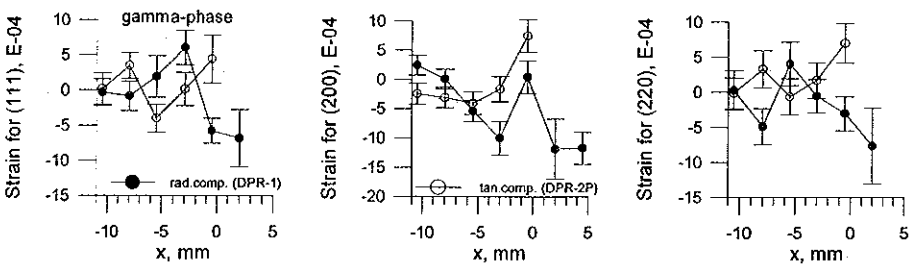

Fig. 13. The dependence of the tangential and radial components of the strain ε on the location of the gauge volume x for the reflexes measured from the investigated sample in the γ-phase with the DPR-1 and DPR-2P detectors.

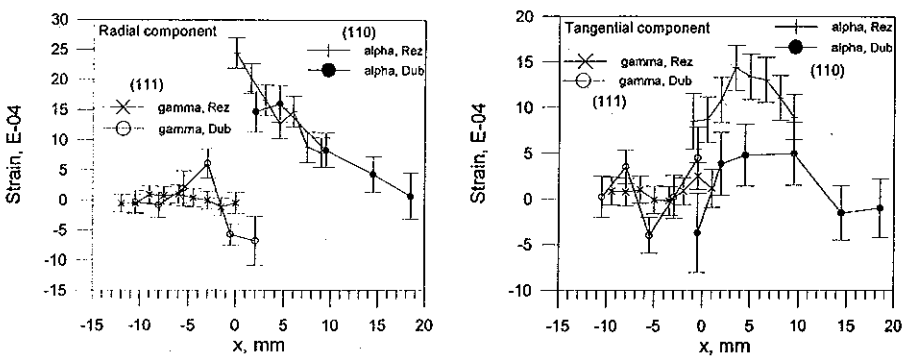

Fig. 14. The dependence of the radial (left) and tangential (right) components of the strain ε on the x location of the gauge volume as measured with the TKSN-400 and HRFD for the investigated sample in the α- and γ-phases.

Since the Bragg peak profile from TKSN-400 is well described by the Gauss distribution, it is interesting to observe the behaviour of the peak widths during the scanning of the sample. Fig. 15 shows the dependence of the peak widths on the gauge volume location when the tangential and radial strain components are measured. Noticeable broadening of the lines near the transitional layer

is the evidence of the presence of III. kind stresses. For some points of the sample, the line profiles were measured more carefully allowing us to analyze them by the Warren-Averbach method (Mignot-Rondon approximation) and determine the mean-square microstrain $\langle\Delta\varepsilon^2\rangle$ [14]. The values of $\langle\Delta\varepsilon^2\rangle$ were used for the calculation of the dislocation density, ρ, which amounted to 10^{14}-10^{16} m^{-2} (Fig. 16). High values of $\langle\Delta\varepsilon^2\rangle$ and the dislocation density reflect strong material damage mainly due to welding in the transition region.

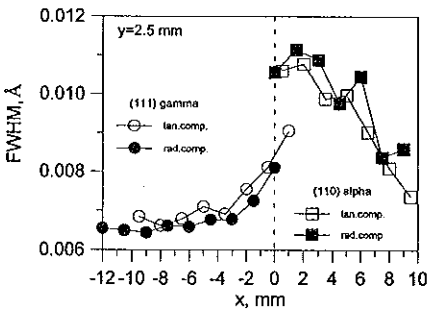

Fig. 15. The (111)- and (110)-peak widths from scanning along the x-axis used to measure the tangential and radial components of the strain tensor.

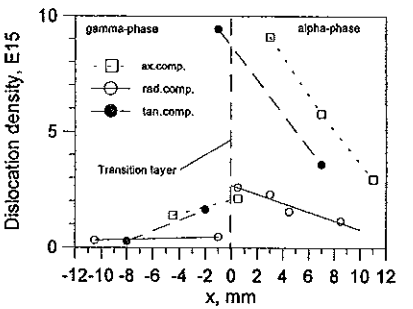

Fig. 16. The dislocation density ρ along the x-axis for three directions of the scattering vector Q.

In Figs. 17 and 18, the HRFD results for (200) reflexes are summarized. Because the gauge volume size in the radial direction was very large, we could not observe, in greater detail, the behaviour of strain near the transitional layer. To do this, we need to improve the space resolution inside the sample by 3 to 4 times.

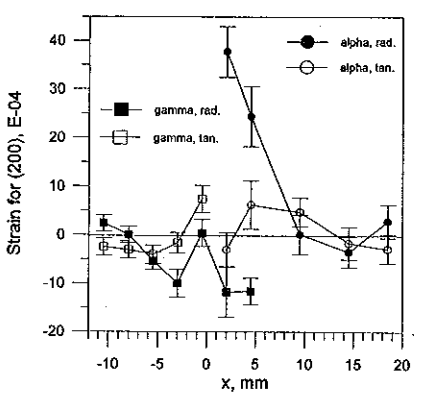

Fig. 17. The dependence of the radial and tangential components of the strain ε on the location of the gauge volume x for (200) reflexes with the orientation factor Γ=0 as measured with the DPR-1 and DPR-2P detectors for the investigated sample in the α- and the γ-phases.

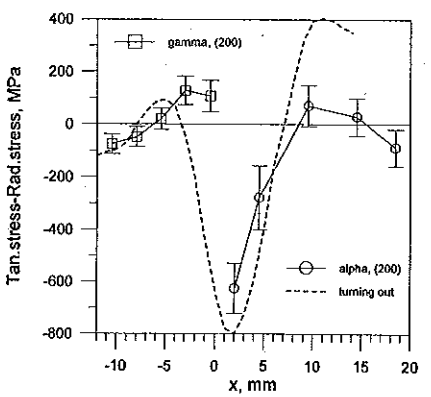

Fig. 18. The dependence of the difference between the tangential and radial stress components, $(\sigma_t - \sigma_r)$, on the location, x, of the gauge volume. The results are shown in comparison with those obtained by the destructive turning out method.

Discussion. In the general case, the obtained data are insufficient for the calculation of residual stresses. However, if assume that the x-,y-, and z-axis (Fig. 2) are the principle axes for the stress tensor of the investigated sample, the components of the tensor can be calculated by the formula (in the elastic model approximation):

$$\sigma_i = \frac{E}{1+\nu}\left[\varepsilon_i + \frac{\nu}{1-2\nu}\left(\varepsilon_r + \varepsilon_t + \varepsilon_a\right)\right],$$

where i = r, t, a indicate the radial, tangential and axial directions of the scattering vector **Q**. Since the axial component was not measured in the HRFD experiments, we can calculate only the difference between the tangential and radial components of the stress tensor:

$$\delta\sigma = \sigma_t - \sigma_r = \frac{E}{1+\nu}\left(\varepsilon_t - \varepsilon_r\right).$$

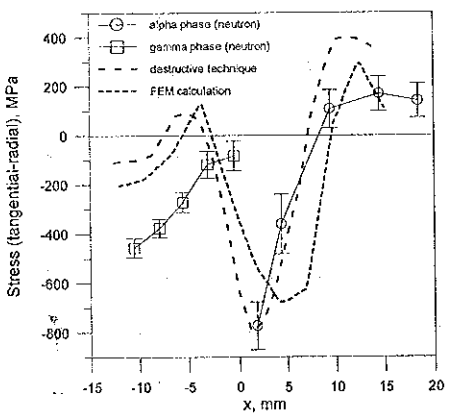

Fig. 19. Comparison of theoretical and corrected experimental stress values for the difference between the tangential and radial components.

In Fig. 18, the stress difference in the tangential and radial directions obtained from the neutron data is shown in dependence on the gauge volume location. Comparing this result with that by the destructive turning out technique applied to an uncut tube, the stress release during cutting has to be accounted for (see Table 2). Assuming that the released stress varied linearly over the interval from the outer to the inner edge and that the radial component did not change essentially during cutting, the residual stress in the uncut tube can be predicted from the neutron diffraction data. The corrected neutron results are shown in Fig. 19. Also, in Fig. 19 the theoretical estimate of the stress state by the finite element method is presented.

For the ferritic part of the tube, good agreement of the neutron result with the theoretical and turning out results can be found. For the austenitic side, disagreement is certainly related to the uncontrollable influence of II. kind microstress on the results of neutron measurements.

4. X-RAY MEASUREMENTS

X-ray diffraction measurements were made with the Seifert diffractometer XRD 3000 PTS-MR using Cr-Kα_1 radiation and a positive sensitive detector. The sample surface near which neutron measurements were done was smoothed and electropolished.

The $\sin^2\psi$-method was applied to determine the distribution of the radial (σ_r) and axial (σ_a) stress components along the radial scan line. If in the sample coordinate system (x,y,z) (see Fig. 2) the scattering vector Q has the angle ψ with axis y and his projection on the analyzing plane (x,z) has the angle φ with the axis x then the strain along Q is equal (see, f.e., [7]):

$$\varepsilon_{\varphi\psi} = \frac{d_{\varphi\psi} - d_0}{d_0} = \frac{1+\nu}{E}\sigma_\varphi \sin^2\psi + \frac{1}{E}\sigma_{33} - \frac{\nu}{E}(\sigma_{11}+\sigma_{22}) + \frac{1+\nu}{E}(\sigma_{13}\cos\varphi + \sigma_{23}\sin\varphi)\sin 2\psi,$$

where $\sigma_\varphi = \sigma_{11}\cos^2\varphi + \sigma_{12}\sin 2\varphi + \sigma_{22}\sin^2\varphi - \sigma_{33}$, σ_{ij} are the components of the stress tensor in the coordinate system (x,y,z). For the Q direction perpendicular to the surface ψ=0:

$$\varepsilon_\perp = \frac{d_\perp - d_0}{d_0} = \frac{1}{E}\sigma_{33} - \frac{\nu}{E}(\sigma_{11}+\sigma_{22}).$$

The difference $\varepsilon_{\varphi\psi} - \varepsilon_\perp$ will not practically change if assume that $d_0 \approx d_\perp$:

$$\varepsilon_{\varphi\psi} - \varepsilon_\perp = \frac{d_{\varphi\psi} - d_\perp}{d_0} \approx \frac{d_{\varphi\psi} - d_\perp}{d_\perp} = \frac{1}{2}\cot\theta_\perp (2\theta_{\varphi\psi} - 2\theta_\perp).$$

We have then:

$$\varepsilon_{\varphi\psi} - \varepsilon_\perp = \frac{1+\nu}{E}\sigma_\varphi \sin^2\psi + \frac{1+\nu}{E}(\sigma_{13}\cos\varphi + \sigma_{23}\sin\varphi)\sin 2\psi.$$

If the shear stresses σ_{13}, σ_{23} are negligible in the volume sampled by the X-ray beam, this equation predicts a linear dependence of $d_{\varphi\psi}$ (or $2\theta_{\varphi\psi}$) vs. $\sin^2\psi$. The stress σ_φ may be found from the slope m_φ of the least-squares curve fit to the experimental data $2\theta_{\varphi\psi}$:

$$\sigma_\varphi = -\frac{1}{2}\frac{E}{1+\nu} m_\varphi \cot\theta_\perp.$$

In the opposite case the so-called ψ-splitting of the dependence $d_{\varphi\psi}$ vs. $\sin^2\psi$ measured for the positive and negative values of ψ will be observed.

For the ferritic part, quite satisfactory linear plots $2\theta_{(211)}$ vs. $\sin^2\psi$ for the (211) reflex were obtained. In Fig. 20, the experimental values $2\theta_{(211)}$ (φ=0) measured in the points x=1.5 and 13.5 mm for the ψ-tilt 0, ±22, ±33, ±42, ±50, and ±60° are exemplified. To recover all components of the strain tensor, the measurements were conducted for the φ-tilt 0, 45, 90°. In Fig. 21, the difference of the radial and axial components σ_{11}-σ_{22}=σ_r-σ_a is shown as a function of the location of the X-ray spot on the sample surface. Good agreement between X-ray data and the results of the turning out method was observed.

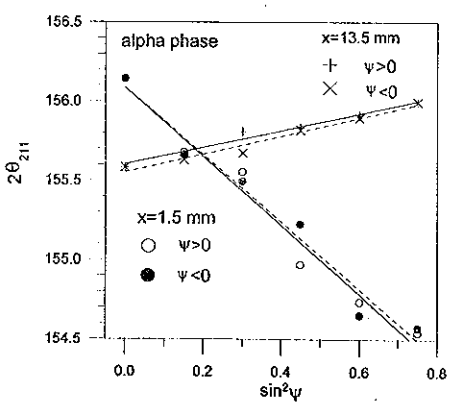

Fig. 20. The dependence of $2\theta_{(211)}$ (φ=0) vs. $\sin^2\psi$ measured for the positive and negative values of ψ for the ferritic part.

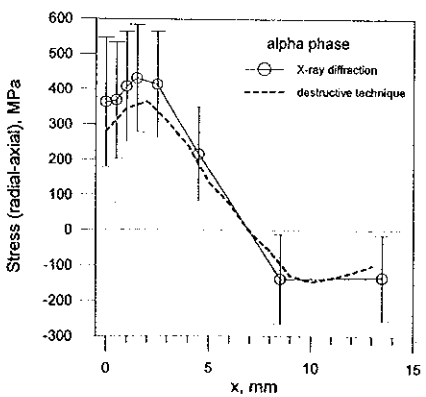

Fig. 21. The dependence of σ_r-σ_a on the coordinate x, where x=0 corresponds to the transition layer.

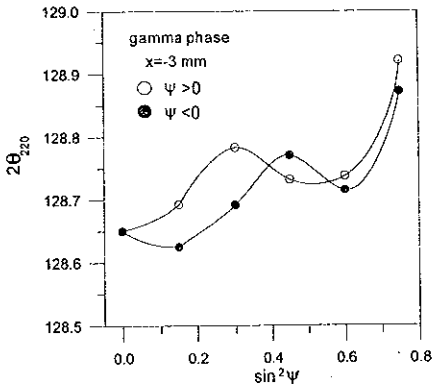

A more complicate situation is observed for the austenitic part. In Fig. 22, the example of the observed plot $2\theta_{(220)}$ vs. $\sin^2\psi$ for the (220) reflex is shown. The determination of stress is not feasible because of strong nonlinearities and the presence of ψ-splitting on this plot. Some special method of data processing is needed to evaluate stresses in this case.

Fig. 22. The dependence of $2\theta_{(220)}$ (φ=0) vs. $\sin^2\psi$ measured for the positive and negative values of ψ for the austenitic part.

5. CONCLUSION

Putting into operation in 1992 of the High Resolution Fourier Diffractometer has allowed to begin realization of the residual stress investigation program in bulk samples for industrial applications [15]. The first neutron diffraction investigations of residual stresses in shape welded tubes yielded satisfactory results. Qualitative, and even quantitative, agreement with the destructive turning out method, as well as with results of the finite element method calculation can be acknowledged. However, in subsequent investigations a more complete analysis of the residual stress state will be carried out. We are planning to measure all three stress components with a larger tube segment using the new 5-axis Huber goniometer on HRFD. For this purpose, the $\sin^2\psi$-method will be applied. In addition, it would be useful to determine the elastic constants by carrying out a tensile test experiment. At the same time, the problem of determination of the parameters of the stress-free reference state has to be solved.

References

[1] K.Kußmaul, F.-W.Schoch, H.Luckow, Welding Journal (1983) 17-24.

[2] K.Berreth, H.Kockelmann, Optimierung der Formschweißtechnik für druckführende und korrosiv beanspruchte Komponenten der chemischen Industrie, Abschlußbericht zum AiF-Forschungsvorhaben Nr. 8954, 1995, MPA Stuttgart.

[3] G.Dobmann, Non-destructive Measurement and Analysis of Residual Stress in and around Welds (a State of Art Survey), Document V 847/87 of the Intern. Institute of Welding, 1987.

[4] G.Dobmann, P.Höller, Non-Destructive Determination of Material Properties and Stresses, 10th Intern. Conf. on NDE in the Nuclear and Pressure Vessel Industries, Glasgow 1990, (Ohio: ASM International), p. 641.

[5] A.J.Allen, M.T.Hutchings, C.G.Windsor, C.Andreani, Adv. in Phys. 34/4 (1985) 445.

[6] M.T.Hutchings, A.D.Krawitz, Measurement of Residual and Applied Stress Using Neutron Diffraction (Dordrecht: Kluwer Academic Publishers and NATO Scientific Affairs Division, 1992).

[7] I.C.Noyan, J.B.Cohen, Residual Stresses (Measurement by Diffraction and Interpretation) (New York: Springer-Verlag, 1987).

[8] V.L.Aksenov, A.M.Balagurov, V.G.Simkin, Yu.V.Taran, V.A.Trounov, V.A.Kudrjashev, A.P.Bulkin, V.G.Muratov, P.Hiismaki, A.Tiitta, O.Antson, The New Fourier Diffractometer at the IBR-2 Reactor: Design and First Results. 12th Meeting of the Intern. Collaboration on Advanced Neutron Sources (ICANS-XII), Abingdon 1993, vol.1, p.124.

[9] M.Vrana, P.Lukas, P.Mikula, J.Kulda, Nucl.Instr.Meth. in Phys.Res. A 338 (1994) 125-131.

[10] V.L.Aksenov, A.M.Balagurov, G.D.Bokuchava, J.Schreiber, Yu.V.Taran, Estimation of Residual Stress in Cold Rolled Iron-Disks from Strain Measurements on the High Resolution Fourier Diffractometer. JINR, E14-95-37, Dubna, 1995.

[11] V.L.Aksenov, A.M.Balagurov, G.D.Bokuchava, J.Schreiber, Yu.V.Taran, Estimation of Residual Stress in Cold Rolled Iron-Disks Using Magnetic and Ultrasonic Methods and Neutron Diffraction Technique, 1994 Fall Meeting of Materials Research Society, Boston 1994, p. 778.

[12] V.B.Zlokazov, V.V.Chernyshov, MRIA - a Program for Full Profile Analysis of Powder Neutron-Diffraction Time-of-Flight (Direct and Fourier) Spectra. JINR, P10-90-315, Dubna, 1990.

[13] L.Pintschovius, Microstresses and Stress Tensors Macrostresses, In: Measurement of Residual and Applied Stress Using Neutron Diffraction, M.T.Hutchings and A.D.Krawitz Eds. (Dordrecht/Boston/London: Kluwer Academic Publishers, 1992), p.115.

[14] P.Lukas, J.Janovec, K.Macek, P.Mikula, P.Strunz, M.Vrana, M.Zaffagnini, Micro Stresses in Welded High-Strength Stainless Steels, 1994 Fall Meeting of Materials Research Society, Boston 1994, p. 777.

[15] V.L.Aksenov, A.M.Balagurov, V.G.Simkin, Yu.V.Taran, V.A.Trounov, V.A.Kudrjashev, A.P.Bulkin, J.Schreiber, On determination of residual stresses with the high resolution Fourier diffractometer at the IBR-2 reactor, Applied Crystallography, Proc. of XVI Confer. (Cieszyn), World Scientific, 1995, p.120.

Received by Publishing Department
on March 17, 1997.